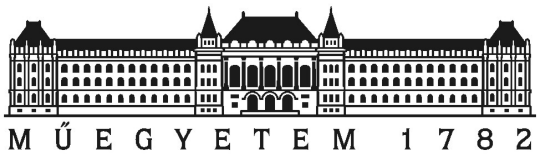

TDK Thesis

Potential MRI contrast agents: PARACEST measurements on lanthanide complexes

Ágner Dorina

Supervisor:

Sophie Laine (*Center for Molecular Biophysics, CNRS*)

Co-supervisors:

Bokor Mónika (*Wigner Research Centre for Physics*)

Simon Ferenc (*Department of Physics, BME*)

Budapest University of Technology and Economics

2015

Contents

Acknowledgements

Firstly, I would like to express my sincere gratitude to my supervisor, Sophie Laine for her patience and motivation. Her guidance helped me in all the time of research and writing of this thesis.

I am grateful to Dr. Jakab Tóth Éva, who provided me an opportunity to join their team as an intern, and who gave access to the laboratory and research facilities. Also, I would like to thank to Célia S. Bonnet for helping me with this thesis.

My sincere thanks also goes to my co-supervisors, Simon Ferenc and Bokor Mónika, for their comments, help and support.

This work was financially supported by the MTA BME Spintronics Research Group (PROSPIN) and by the European Research Council Grant Nr. ERC-259374-Sylo.

1 Introduction and Motivation

One of the most often used imaging methods in the modern medical diagnostics is Magnetic Resonance Imaging (MRI). With MRI, the imaging plane can be optimized for the studied anatomic area. MR spectroscopy has enormous potential for providing information about the biochemistry and metabolism of tissues. As an imaging technology, MR has advanced over the past ten years, but it continues to evolve and new capabilities will likely be developed.

Among the medical applications of MRI, using contrast agents became indispensable, as they are used to enhance the visibility of internal body structures. Thus this subject became one of the most popular surfaces between doctors, chemists, biologists and also physicists.

In order to detect enzymatic activities, "smart" contrast agents have been developed, the lanthanide complexes I studied represent some of these. In order to find out, PARACEST (Paramagnetic Chemical Exchange Saturation Transfer) measurements were performed. The main advantage of the PARACEST contrast agents is the ability to switch them on and off, so more than one agents can be used in one experiment.

The main purpose of the project which is lead by Dr. Eva Jakab Toth at the Center for Molecular Biophysics, CNRS Orleans, is to find MRI contrast agents for detecting enzymatic activity. In this work, we are interested in detecting amidase activity. Enzymes are proteins that control almost all of the chemical reactions in the human body. An amidase is an enzyme that catalyzes the hydrolysis of an amide.

My work in the team was to study different complexes before enzymatic cleavage, to see if they have proper PARACEST effects. In this thesis, I discuss some previous work from the team's work, in order to compare the results measured before and after enzymatic cleavage.

Knowledge of the exchange rates of labile protons is very important in the study of biomolecules, for example it provides information about local and global flexibility, allows derivation of secondary structure as well as assessment of interaction interfaces, and enables features of great interest such as folding and unfolding of biomolecules to be followed [1]. Hence, our intent was to calculate the proton-exchange rate (k_{ex}) between the studied molecules and the solvent (typically water). In order to determine the k_{ex} values, QUESP and QUEST measurements were made at different pH values of the samples.

2 Theoretical background

2.1 Principles of NMR and MRI

2.1.1 NMR spectroscopy

NMR (Nuclear Magnetic Resonance) is a widely used spectroscopic method for studying materials and molecular physics, it is used for example in medical researches and in MRI (Magnetic Resonance Imaging).

The base phenomenon is the following: nuclei in a magnetic field absorb and re-emit electromagnetic radiation. The process has a purely quantum physical nature, but here, an equivalent, classical representation is used.

If the sample is taken into a static magnetic field (B_0, which is in the direction of the z axis), the nucleus obeys the Larmor relation and precesses about the field. The frequency of the precession is the Larmor frequency: $\omega_L = \gamma B_0$, where γ is so-called gyromagnetic ratio, which is unique to each isotope.

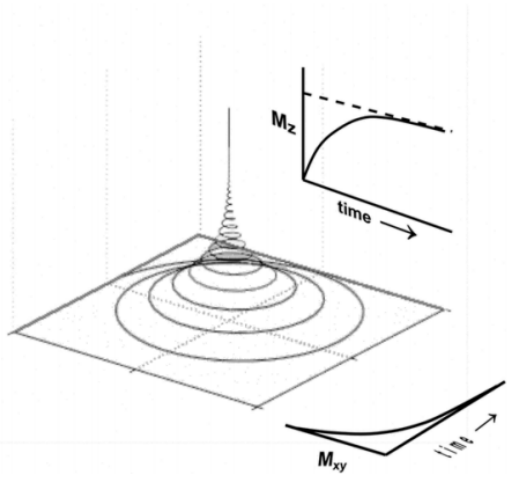

Figure 1: The relaxation of the magnetic moment vector [2]

To irradiate the magnetic moments, short pulses of rotating magnetic fields, perpendicular to the z axis are used, they cause displacement of the magnetic moments from their equilibrium, direction towards the x-y plane. The proceeding relaxation is then detected. This relaxation follows an exponential decay with characteristic time T_1 along the z axis and T_2 in the x-y plane (Figure 1), the motion of the magnetic moment vector of the nucleus ($M(t)$) can be described by the Bloch-equations [3]. The x and y components of the resultant magnetic moment are detected. In case of off-resonance detection, the signal is an oscillating function with an exponential envelope [2].

Free Induction Decay

FID (Free Induction Decay) sequence consists of a single $\pi/2$-pulse, which rotates the magnetic moments by 90°. The characteristic time of the following exponential decay is T_2^*, this is the so-called reversible relaxation time. It is caused by the magnetic field inhomogeneities, which can cause the decoherence of the moments, this decoherence is usually much faster than the spin-spin relaxation of the individual spins.

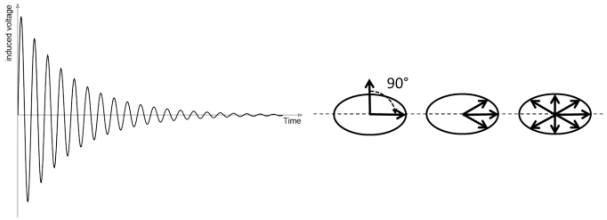

Figure 2: A FID signal and the decoherence of the magnetic moments [2]

Spin-echo

The decoherence in the FID sequence is a process that can be reversed, by applying a π-pulse. If the inversion pulse is applied after a period (τ) of dephasing, the inhomogeneous evolution will rephase to form an echo at time 2τ (Figure 3). In simple cases, the intensity of the echo, relative to the initial signal is given by $e^{-2\tau/T_2}$, where T_2 is the time constant for spin-spin relaxation (the transverse relaxation time), thus during the Spin-echo sequence, T_2 relaxation is inevitable.

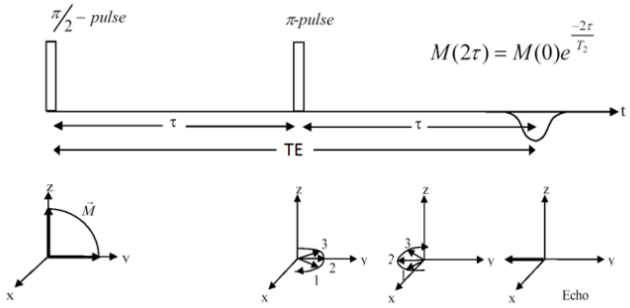

Figure 3: The schematic representation of the spin-echo sequence [2]

2.1.2 The basics of MRI

Magnetic resonance (MR) is a dynamic and flexible technology that allows one to tailor the imaging study to the anatomic part of interest and to the disease process being studied. With its dependence on the more biologically variable parameters of proton

density[1], longitudinal relaxation time (T_1), and transverse relaxation time (T_2), variable image contrast can be achieved by using different pulse sequences and by changing the imaging parameters [4].

An MRI scanner forms a strong magnetic field around the area to be imaged. In most medical applications, protons in tissues containing water molecules are used to create a signal that is processed to form an image.

First, an oscillating magnetic field is temporarily applied to the sample at the appropriate resonance frequency. The excited hydrogen atoms emit a radio frequency signal (RF) which is measured by a receiving coil. The radio signal can be made to encode position information by varying the main magnetic field using gradient coils. The contrast between different tissues is determined by the rate at which excited atoms return to the equilibrium state. Signal intensities on T_1, T_2, and proton density-weighted images relate to specific tissue characteristics.

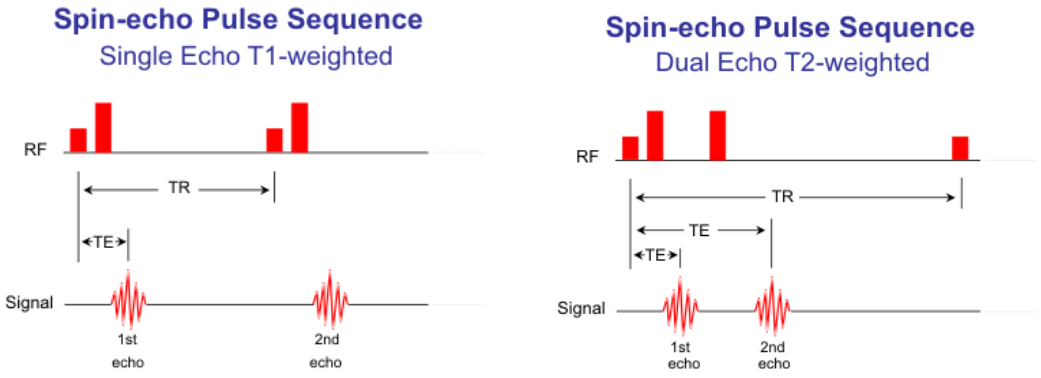

Figure 4: Schemes of T_1-weighted (left) and T_2-weighted (right) spin-echo sequences [4]

The contrast on the MR image can be manipulated by changing the pulse sequence parameters. A pulse sequence sets the specific number, strength, and timing of the RF and gradient pulses. The two most important parameters are the repetition time (TR) and the echo time (TE). TR is the time between consecutive 90° RF pulses, TE is the time between the initial 90° RF pulse and the echo. The most common pulse sequences are the T_1-weighted and T_2-weighted spin-echo sequences (Figure 4). The T_1-weighted sequence uses a short TR and a short TE (TR $<$ 1000 ms, TE $<$ 30 ms). The T_2-weighted sequence uses a long TR and a long TE (TR $>$ 2000 ms, TE $>$ 80 ms). The T_2-weighted sequence can be employed as a dual echo sequence [4].

[1]Proton density is the concentration of protons in the tissue in the form of water and macromolecules (proteins, fat, etc).

2.1.3 Traditional contrast agents

MRI contrast agents are a group of contrast media used to improve the visibility of internal body structures in magnetic resonance imaging. The most commonly used compounds for contrast enhancement are gadolinium-based.

Paramagnetic metal ions possessing one or more unpaired electrons have permanent magnetic moments, such as Mn^{2+} and Gd^{3+} ions, which have five or seven unpaired electrons. In water, there is a dipolar magnetic interaction, between the electronic magnetic moment of the paramagnetic metallic ion and the magnetic moment of the proton of the surrounding waters molecules. These interactions are characterized with a diminution in both longitudinal (T_1) and transverse (T_2) relaxations times of the water protons. Due to their undesirable biodistribution and their high toxicity, paramagnetic metallic ions, like Gd^{3+} cannot be used as contrast agents. To avoid these drawbacks, chemical chelates showing high thermodynamic and high kinetic stability are used to complex the metallic paramagnetic ions. Dotarem an Magnevist are the most known contrast agents as they are commonly used in clinical MRI experiments (Figure 5) [5].

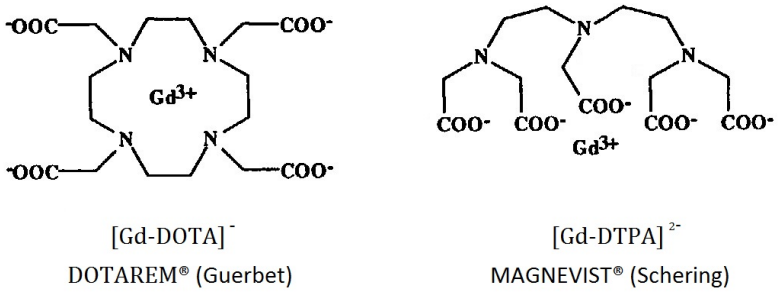

Figure 5: Dotarem and Magnevist commercial contrast agents

The efficiency of the MRI contrast agents is measured with their relaxivity values (r_1 and r_2), which indicate their ability to decrease respectively the T_1 or T_2 relaxation times of the protons of the surrounding water in the targeted tissue. The relaxivity effects of these agents results mostly from their inner sphere mechanism. r_1 depends on three parameters: q, the number of water molecules coordinated to the metal ion, t_r, the rotational correlation time and k_{ex}, the water exchange rate (shown in Figure 6).

In the MRI images an increase of the relativity will be translated into an increase in the contrast image.

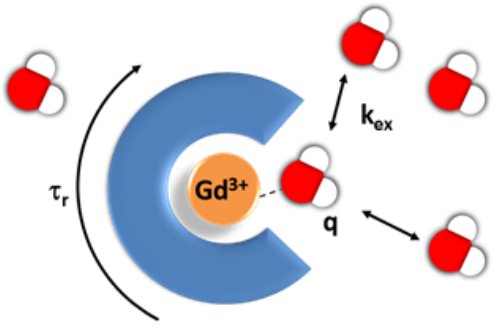

Figure 6: Inner sphere mechanism of a traditional contrast agent

2.2 CEST and PARACEST

2.2.1 CEST effect

CEST is an acronym for Chemical Exchange Saturation Transfer. This method relies on the fact that the resonance frequencies of protons in the solute and the solvent can be different (it is often the case due to the differing chemical environment) and that they are in a chemical exchange process where the protons physically move from the solute to solvent and back [6].

In a system, where there are two exchanging protons: Pool A and Pool B, a saturation via selective RF irradiation at Pool B's frequency also has an effect on the protons in Pool A. This means that when the system is interrogated by a 90° pulse, not only the signal intensity of Pool B is almost completely absent, but the intensity of Pool A is also decreased [7]. The next image is a schematic representation of the experiment.

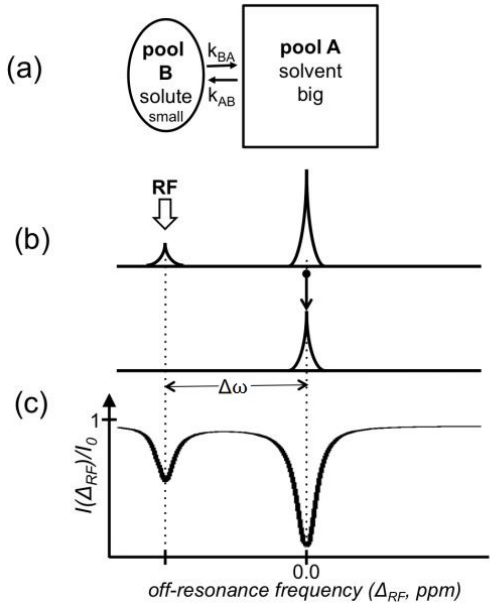

Figure 7: CEST experiment: a) Pool A is in exchange with Pool B; b) RF is applied on-resonance with pool B, the signal of Pool A also decreases; c) CEST spectra: normalized water intensity (I/I_0) as a function of frequency of the saturating RF [6]

In order to an effect to be observed, the protons must have magnetically distinct environments, and the exchange process must be slow on the NMR timescale. This means that the frequency difference between the two chemical environments ($\Delta\omega$) must be greater than the proton-exchange rate (k_{ex}) [7]:

$$\Delta\omega \geq k_{ex}$$

The CEST process is in competition with the relaxation, if the longitudinal relaxation rate (R_1) of Pool B is faster than k_{BA} ($k_{ex} = k_{AB} + k_{BA}$, the transition rate of a magnetization leaving Pool B, Figure 7), the system will relax back to its equilibrium, before the exchange can transfer the saturation [7].

During a CEST measurement, the program usually sweeps through an interval, changing the pre-saturation frequency, but the frequency of the $\pi/2$ pulse (the acquisition pulse) is always the same (the solvent's, in this case it is the protons's of the water). In order to get the CEST spectra, we have to normalize the signal intensity, with the water's maximum intensity (M_s/M_0 or I/I_0). The plot of this (usually in percentage) as a function of the off-resonance saturation frequency (ppm) is called the CEST spectra, it can be seen in Figure 7c.

2.2.2 PARACEST complexes as contrast agents

Types of CEST agents

The following summary about the types of CEST agents is based on the article by Vinogradov et al. [6].

In recent years a great variety of molecules were proposed to serve as CEST agents, for example the followings, classified by the nature of the solute:

- Diamagnetic CEST (DIACEST): the chemical shift is typically within 5 ppm from water, which makes the detection hard, because of the partial saturation of the bulk water protons.
- Paramagnetic CEST (PARACEST): The chemical shift is typically larger than in the case of DIACEST agents (more details further on).
- Using liposomes (LIPOCEST): increasing the number of exchanging groups (protons) per agent also increases the CEST effect. The LIPOCEST systems were developed based on this phenomenon. Very high sensitivities can be achieved by the use of liposomes.
- Using hyperpolarized gases (HYPERCEST): the principles of CEST have been used in conjunction with hyperpolarized Xe biosensors.

PARACEST: Origins and advantages

In early 2000, paramagnetic lanthanide complexes were introduced as CEST agents. The highly shifted bound water protons, or the amide or hydroxyl protons of the ligand on the agent molecules can be selectively pre-saturated, and the saturation can be transferred

to free water via chemical exchange (Section 2.2.1). PARACEST agents exhibit a wide range of exchange rates, the fastest ones allow the use of lower concentrations of the agents [6]. The maximum permissible exchange rate is determined by the frequency difference between the two pools (as mentioned earlier): the larger the value of $\Delta\omega$, the faster the permissible k_{ex}. The effectiveness of an agent can be improved by maximizing both parameters (k_{ex}, $\Delta\omega$) [7].

One further advantage of PARACEST agents is that the selective RF pulse is applied far from the water resonance frequency, which reduces the direct RF saturation transfer effects [6].

Because of the similar valence and coordination chemistry of the lanthanides, they are virtually identical along the series, isostructural complexes can be prepared with most of the lanthanide ions and any given ligand system. Hence the hyperfine shift characteriscics and relaxation properties of a PARACEST agent can be tuned according to the choice of lanthanide ion. This enables to administer simultaneously more than one PARACEST agent, and each of these agents could be activated separately [7]. With these agents, images with contrasts based on other mechanisms can be measured in the same scan session [6].

A schematic, significant representation is shown in the article written by Woods et al. [7]: the selective irradiation of four samples; one containing Eu ($+50\,ppm$), and one Tb ($-600\,ppm$) complex in water, one containing a mixture of both and one only water. The graph of the simulation is shown in Figure 8.

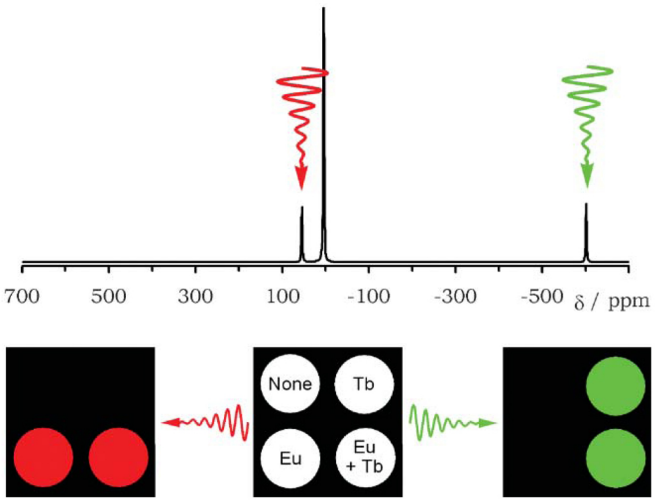

Figure 8: Simulated ^{1}H NMR spectra showing the coordinated water proton resonances of four samples. It is shown that each complex may be activated selectively regardless of the presence or absence of an other complex. [7]

There are many applications of the PARACEST agents, for example they can be pH or temperature sensors, or used to detect enzymatic activity (as it will be demonstrated later). The use of multiple agents could be useful in cell tracking experiments, or we could simultaneously detect more than one parameter at the same time [7]. Some types of PARACEST agents are considered to be "smart", because they alertly respond to changes in their molecular environments [8].

3 Experimental techniques

NMR and PARACEST spectra were recorded on a Bruker Avance III HD 400, equipped with a BBFO probe 5 mm (showed in Figure 9), which is located in Center for Molecular Biophysics (CBM) CNRS, Orléans, France. The spectra were recorded in H_2O / D_2O (90 : 10) typically at 300 K. Before each experiment, the probe was tuned, the magnet shimmed and the samples were locked using D_2O.

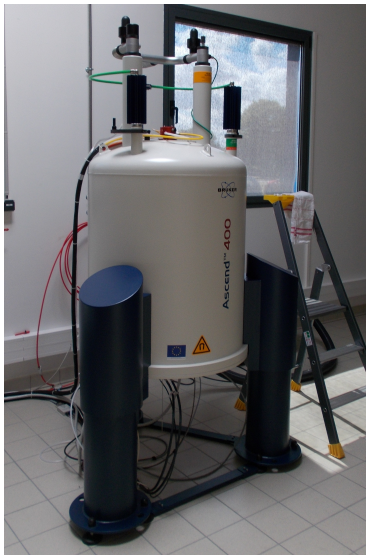

Figure 9: The used 9.4 T NMR magnet

For a single PARACEST spectra, the saturation power value was typically 10 mW, the irradiation delay was kept at 3 s and they were measured in a wide frequency range: from −150 to 150 ppm, each ppms.

Besides the CEST experiment, the ^{1}H NMR spectrum of each sample was measured, using a presaturation sequence on the water signal frequency.

3.1 Measuring methods

This section is based on the article by Vinogradov et al. [6].

Basic principles

CEST is a family member of a group of NMR experiment known as Saturation Transfer (ST). The saturation transfer experiment is one of the oldest NMR experiments[2].

[2]Overhauser purposed saturation of the electron line to modulate nuclei relaxation and magnetization in [9].

In the simplest description of the system, showed in Figure 7, there are no scalar couplings between the two pools and no coherent interactions, and the system can be described by the modified Bloch equations (the following equation).

ST can occur via two types of interactions: dipolar mediated cross relaxation through space and chemical exchange. Further on only the chemical exchange will be discussed. The dynamics can be described by a set of Bloch equations modified for exchange and the presence of RF. The equations for the two-pool model can be written as follows.

$$\frac{d}{dt}\begin{pmatrix} M_x^A \\ M_y^A \\ M_z^A \\ M_x^B \\ M_y^B \\ M_z^B \end{pmatrix} = \begin{pmatrix} -\rho_{2A} & -\Delta_A & 0 & k_{BA} & 0 & 0 \\ \Delta_A & -\rho_{2A} & \omega_1 & 0 & k_{AB} & 0 \\ 0 & -\omega_1 & -\rho_{1A} & 0 & 0 & k_{BA} \\ k_{BA} & 0 & 0 & -\rho_{2B} & -\Delta_B & 0 \\ 0 & k_{AB} & 0 & \Delta_B & -\rho_{2B} & \omega_1 \\ 0 & 0 & k_{AB} & 0 & -\omega_1 & -\rho_{1B} \end{pmatrix} \begin{pmatrix} M_x^A \\ M_y^A \\ M_z^A \\ M_x^B \\ M_y^B \\ M_z^B \end{pmatrix} + \begin{pmatrix} 0 \\ 0 \\ R_{1A}M_0^A \\ 0 \\ 0 \\ R_{1A}M_0^B \end{pmatrix}$$

where $\rho_{1A} = R_{1A} + k_{AB}$, $\rho_{2A} = R_{2A} + k_{AB}$; $\rho_{1B} = R_{1B} + k_{BA}$, $\rho_{2B} = R_{2B} + k_{BA}$, $\Delta_{A,B} = \omega_{A,B} - \omega_{RF}$, ω_{RF} and ω_1 are the frequency and the amplitude of the RF irradiation (in rad/s units). k_{ex} is the proton-exchange rate ($k_{ex} = k_{AB} + k_{BA}$), where k_{AB} is the transition rate of a magnetization leaving Pool A, Δ_A is the chemical shift offset from RF frequency for Pool A, R_{1A} and R_{2A} are the spin lattice and the transverse relaxation rates of Pool A. Similar definitions apply for Pool B.

Experiments

The two main types of saturation-transfer experiments are: steady-state and transient. The steady-state experiments refer to the state in which the system does not change further and the state is time independent (the derivates in the modified Bloch equations are all zero). The transient experiment refers to the case when the system is still changing, and the explicit time dependence cannot be ignored. The general scheme of saturation transfer experiment is shown on Figure 10: blue boxes indicate RF irradiation blocks, white boxes indicate acquisition blocks (ACQ: spectroscopy or imaging). Dotted lines mark repetition time (TR) that include saturation time, acquisition time and relaxation delay before saturation. In steady-state experiments, the duration of the saturation (T_s) is much longer than T_1 (T_s,$TR >> T_1$). In segmented steady-state experiment $TR < T_1$, and the whole experiment is repeated many times thus reaching a steady-state around experiment number n, such that $nTR >> T_1$. In transient experiments $T_s < T_1$. In contrast to segmented steady-state experiments $TR >> T_1$. Thus, if the experiment is

repeated again there is no memory of the previous experiment and no steady-state is created [6].

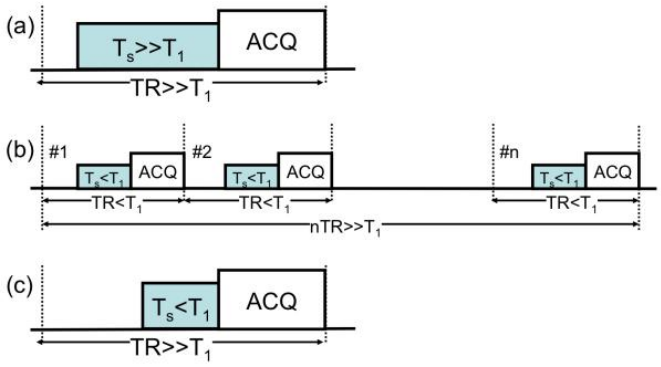

Figure 10: Schematics of Saturation Transfer experiments, a) Steady-state ST experiment, b) Segmented steady-state experiment, c) Transient experiment [6]

3.2 QUEST and QUESP

The two MRI-compatible approaches to measure the proton exchange rate are: quantifying the exchange rate using saturation time (irradiation delay time) (QUEST) dependence and quantifying exchange using saturation power (QUESP) dependence [10].

During a QUEST measurement, more PARACEST spectra were collected by varying the delay time and keeping the power constant. The duration of the saturation pulse was always between 0.25 s ad 4 s, altogether 12 spectra (12 time values) were measured, with each QUEST measurement. The time series were taken at one saturation power value: 10 mW (this corresponds to 1082.25 Hz).

The QUESP sequence is almost the same as QUEST, but in this case, the saturation power was varied, and the irradiation delay time was kept constant (at 3 s). There were typically 19 power values, from 0.07 mW to 30 mW.

From the QUEST and QUESP measurements, we can calculate the proton-exchange rate between the molecules and the water. One can take the minimum values of the PARACEST effect from each spectra (separately QUEST and QUESP), and plot them as a function of the time and power, then the equations (1)-(3) can be fitted to them.

3.3 Samples

The potential contrast agents, I studied, have the same structure, but the molecules contain different lanthanides in their chelating moeity. Figure 11 shows the structure of the molecules. In the figure, the agent's only exchangeable proton and the amidase

substrate can be seen. I investigated the CEST effect for the first molecule shown by varying the lanthanide ion.

In the remaining sections, I used the following notation for the molecules: the symbol of the lanthanide, with an 'L', standing for "Ligand" (meaning that the metal is complexed in the ligand). For example: EuL, HoL, and so on.

Before enzymatic cleavage the substrate of the targeted enzyme is linked to the complexing moiety to an amide group which has one labile proton, after enzymatic cleavage the substrate is gone and an amine group with two labile protons is left. So we expect a change in the PARACEST properties of the two molecules.

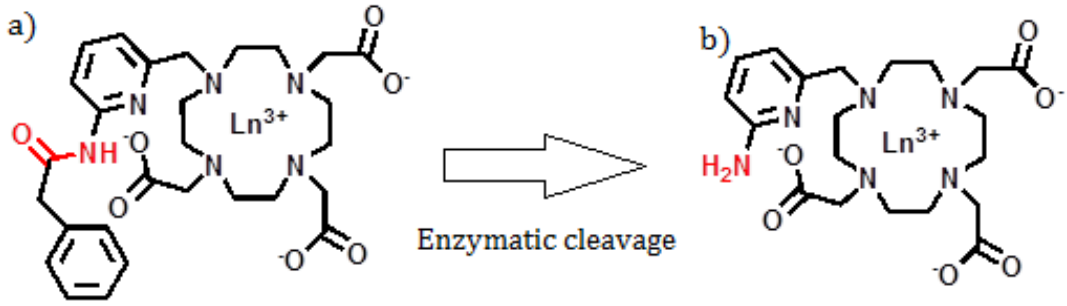

Figure 11: The structure of the molecule before (a) and after (b) enzymatic cleavage

All of the studied molecules were made in the Institut de Chimie des Substances Naturelles UPR CNRS, France. To make the solutions H_2O was added, the concentration of the contrast agents was 20 mM, with about 5 % D_2O content (for the locking). I set the pH to 7.

The measurements done in this work were performed in order to characterize different lanthanide complexes of the molecule before enzymatic cleavage.

3.4 Methods for calculating the proton-exchange rate

Several methods are available to estimate the k_{ex} (the proton-exchange rate), I will use three of them in this thesis, presented by Chauvin et al. in [11]. These methods determine the proton-exchange rate from the delay time and saturation-power dependency of the intensity of the water proton (QUEST and QUESP data).

The first one uses the time, I fitted this equation to each data series from the QUEST measurements.

$$1 - \frac{M_s}{M_0} = 1 - \left(\frac{1}{1 - k_{ex}\chi_{CA}T_1} + \frac{k_{ex}\chi_{CA}T_1}{1 + k_{ex}\chi_{CA}T_1} e^{-(1+k_{ex}\chi_{CA}T_1)t_{sat}} \right) \tag{1}$$

where T_1 is the longitudinal relaxation time, χ_{CA} is the fractional concentration of exchangeable protons of the contrast agent, t_{sat} is the saturation time, $\frac{M_s}{M_0}$ is the minimum value of the spectra in the place of the PARACEST effect. (M_s is the signal intensity, M_0 is the water's maximum intensity.)

The second equation can be applied assuming that the steady state is reached upon the saturation of the solute, this one is used for the power dependent measurements.

$$1 - \frac{M_s}{M_0} = \frac{k_{ex}\alpha\chi_{CA}}{R_{1W} + k_{ex}\chi_{CA}}\left[1 - e^{-(R_{1W}+k_{ex}\chi_{CA})t_{sat}}\right] \tag{2}$$

where α is the saturation efficiency, which can be expressed as follows.

$$\alpha = \frac{\omega^2}{\omega^2 + pq}$$

$$p = R_{2S} + k_{ex} - \frac{k_{ex}^2\chi_{CA}}{R_{2W} + k_{ex}\chi_{CA}}$$

$$q = R_{1S} + k_{ex} - \frac{k_{ex}^2\chi_{CA}}{R_{1W} + k_{ex}\chi_{CA}}$$

where ω is the pulse power (given in Hz), $R_{1,2S}$ and $R_{1,2W}$ are the longitudinal and the transverse relaxation rates of the solute and the bulk water, respectively in the saturated state.

The last expression is called the "omega plot", a concentration independent method, so it can be really useful in some cases. This equation was first presented by Dixon et al. in [12].

$$\frac{M_s}{M_0 - M_s} = \frac{55.5}{c}k_{ex}R_{1W}\left(\frac{1}{k_{ex}^2} + \frac{1}{\omega_1^2}\right) \tag{3}$$

where ω_1 is the amplitude of the radio-frequency applied for the saturation pulse (given in Hz). $\frac{M_s}{M_0-M_s}$ is inversely proportional to ω_1, thus the next expression is true (assuming that k_{ex} is much higher than the relaxation rates).

$$-\frac{1}{k_{ex}^2} = \frac{1}{\omega_1^2}$$

4 Results and Discussion

4.1 PARACEST spectra of lanthanide complexes

The first goal was to explore whether there are any PARACEST effects for all the lanthanide complexes. Hence I measured the PARACEST spectra of all samples. The following figure shows the spectra of six complexes. The observed effects are quite significant for these species, but for the other two (PrL and NdL), no detectable effects could be seen within the examined range. As it is represented in the graph, the molecules have PARACEST effects at different frequencies. These can also be found in Table 1.

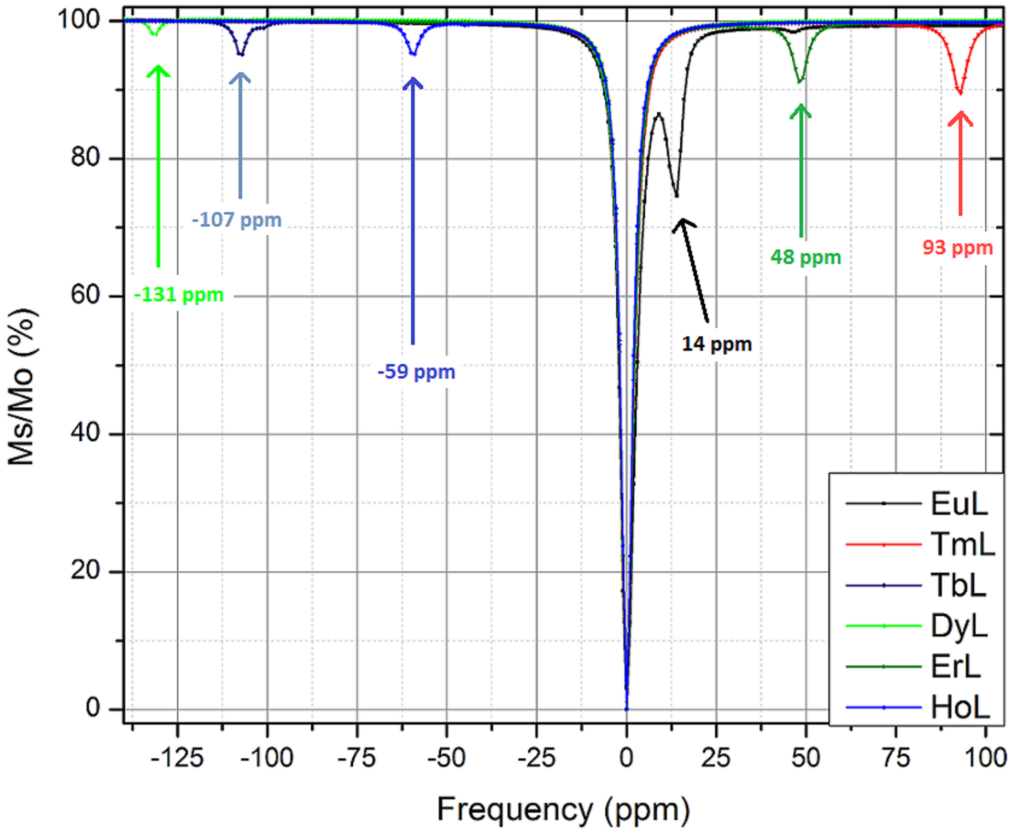

Figure 12: PARACEST spectra of six different samples, the frequencies of the effects indicated (pH 7, 20 mM, 300 K)

Lanthanide complexes	PrL	NdL	EuL	TbL	DyL	HoL	ErL	TmL
Frequency (ppm)	-	-	14	-107	-131	-59	48	93

Table 1: The frequencies of the CEST effects

The CEST frequency is one of the characteristics of the lanthanides, the size of the effect can be varied within limits, for example with varying the pH, the temperature or the concentration. In order to analyze the effects, I ran QUESP and QUEST sequences. To get more precise results, I measured the points more frequently, however to save some time, I set the boundaries depending on the PARACEST-effect's frequency, so the boundaries of the spectra are different in each case.

If we look at the QUESP spectra of EuL, the curve measured at low pH values, with low powers shows that there are two effects with just a few ppm difference and also one near the water signal (Figure 6b).

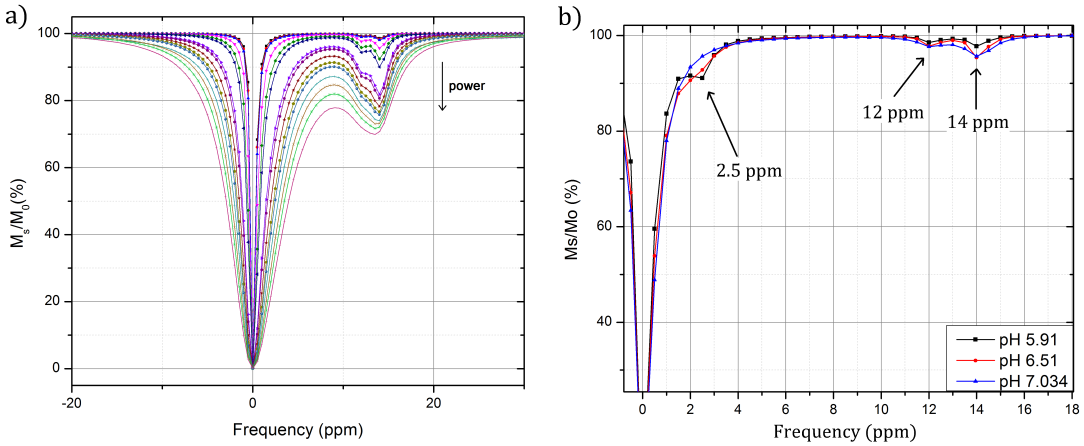

Figure 13: CEST spectra can be examined better with QUESP measurements: a) QUESP measurements of EuL at pH 7 (20 mM, 300 K) b) EuL at three different pH values (20 mM, 300 K), measured with low power. Effects close to each other can be seen separately in both graphs.

The appearance of more than one effect and only one labile proton on the contrast agent structure is due to the presence of different isomers. Thus the explanation of the phenomenon seen is the following: during preparation, the molecule formed three different isomers, each with different CEST effects. In order to calculate the k_{ex} values, the concentrations of the isomers are needed to be known, they can be determined from ^{1}H NMR spectra measured at different temperatures (Figure 14). Since the frequencies are so close to each other, the signals are superimposed and the intensities of the two components cannot be obtained separately, their sum is available only, so it is not possible to determine the k_{ex} in this case.

The spectra at different temperatures (Figure 14) shows that the number of peaks increases by decreasing the temperature, which confirms the presence of different isomers

in the solution. Furthermore, by counting the number of signals, it can be seen that at least three isomers are present in the solution. (We expect around 20 signals at all temperatures, and found around 50 at 278 K).

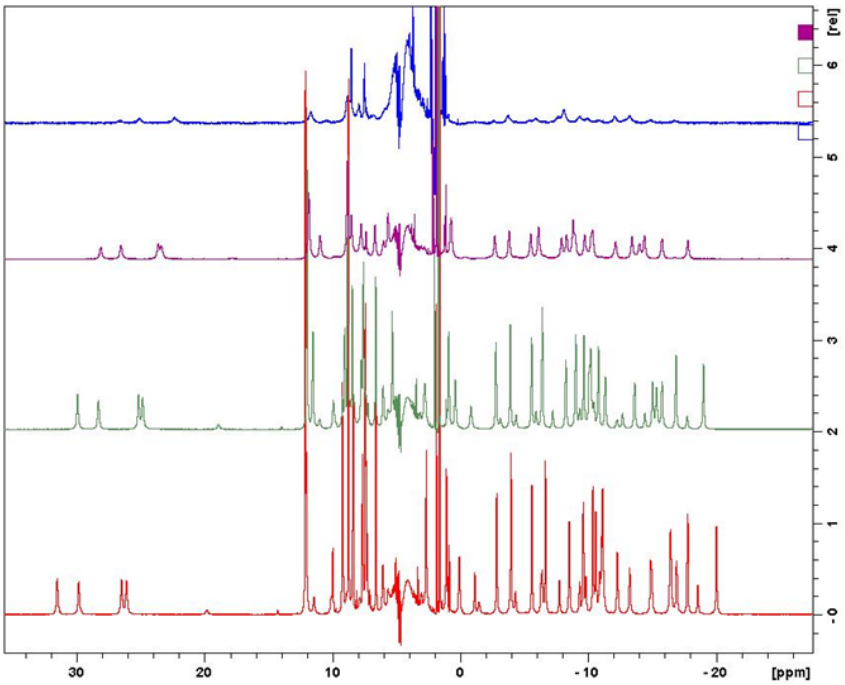

Figure 14: ^{1}H NMR spectra of EuL (20 mM, pH 7.4) at 313 K (blue), 300 K (purple), 288 K (green) and 278 K (red).

The next task was to characterize the effects. Thus I changed the pH of the solutions, I measured the PARACEST spectra and I performed the QUEST and QUESP experiments (the same protocol, as before). I repeated the measurements at five different pH values. I managed to finish the examination of three different complexes (EuL, ErL, TmL, these have the biggest CEST effects), but for Dy and Tb complexes, the CEST effects were so small that the k_{ex} cannot be investigated.

Figure 15 represents the pH dependence of the CEST effect. As it is shown in the graph, increasing the pH value also increases the CEST effect's strength, within limits. The pH shifts the balance between the solute and the solvent, thus it influences the speed of the chemical exchange.

As it was mentioned before, from the QUEST and QUESP measurements, the proton-exchange rate (k_{ex}) can be determined. I examined the complexes at five different pH values, and I calculated each k_{ex} value.

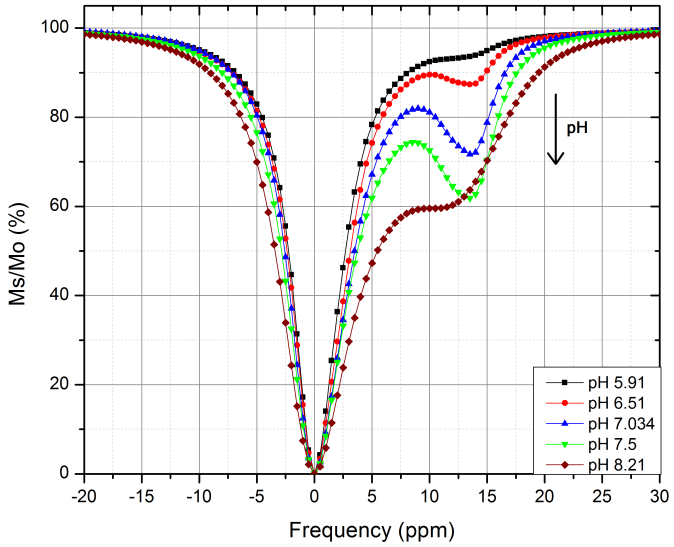

Figure 15: PARACEST spectra of EuL at five different pH values

4.2 ErL complex

At pH 6.06, the CEST effect is very weak, so the calculated k_{ex} value would not be reliable, hence this pH will not be considered in the k_{ex} calculation (the curve is not shown in the QUESP graph).

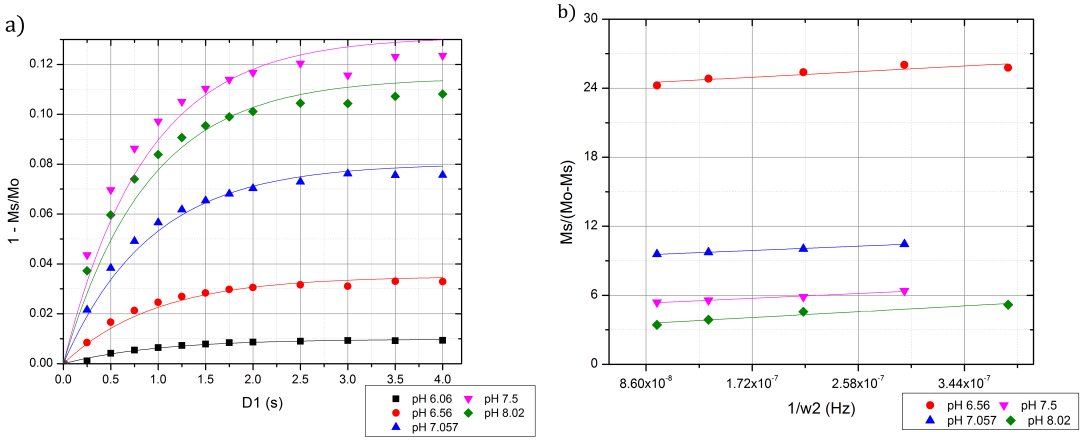

Figure 16: Experiments on ErL complex (20 mM, 300 K): a) QUEST curves, fitted with equation (1). b) Omega plots, fitted with equation (3).

In Figure 16, the outcomes of the QUEST and QUESP (the omega plot) measurements on ErL complex can be seen, with the fitting of equations (1) and (3). The equation, used

for the omega plot was fitted only to the highest powers. The k_{ex} values are listed in Table 2. Figure 17 shows the results of the other method (Equation (2)) for calculating the k_{ex} from the QUESP curves (of other samples), but the error of the fitting is too large, and this is the same for the rest of the curves, so this method will not be used for calculating the k_{ex}.

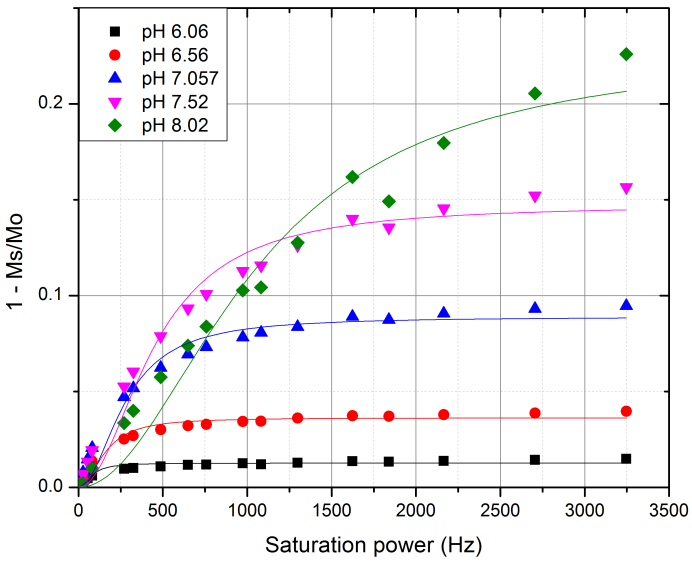

Figure 17: Experiments on ErL complex(20 mM, 300 K): QUESP curves, fitted with equation (2).

		Omega plot method	QUEST method		
pH	Frequency (ppm)	k_{ex} (s^{-1})	k_{ex} (s^{-1})	$\overline{k_{ex}}$ (s^{-1})	Deviation (s^{-1})
6.56	48.5	531	484	508	33
7.057	48.5	815	688	752	90
7.5	48.5	1088	997	1042	64
8.02	48.5	1008	1400	1204	277

Table 2: The proton-exchange rate values of ErL complex (20 mM, 300 K), calculated with QUEST and omega plot methods.

4.3 TmL complex

The outcomes of the QUEST and QUESP (the omega plot) measurements on TmL complex can be seen on Figure 18, the fitted equations were: (1) and (3). The equation,

used for the omega plot was fitted only to the highest powers. The k_{ex} values are listed in Table 3.

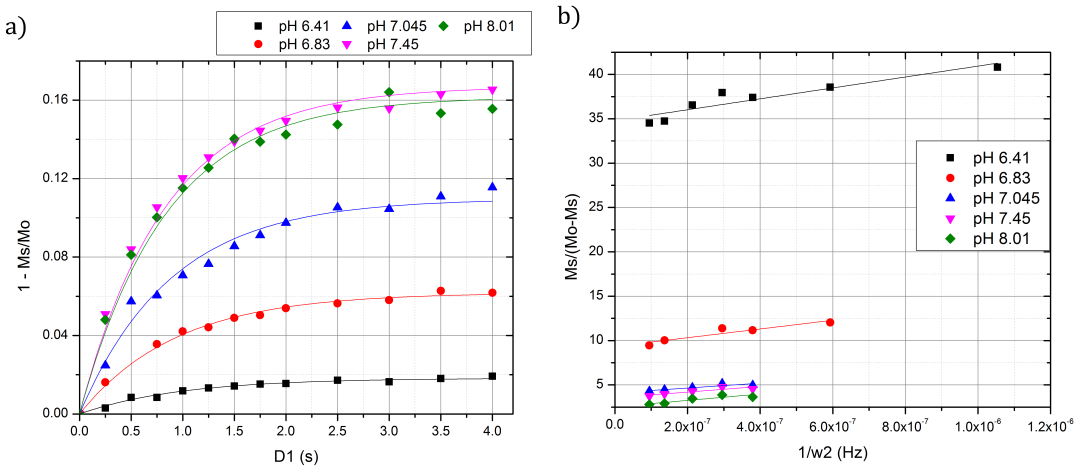

Figure 18: Experiments on TmL complex (20 mM, 300 K): a) QUEST curves, fitted with equation (1). b) Omega plots, fitted with equation (3).

		Omega plot method	QUEST method		
pH	Frequency (ppm)	k_{ex} (s^{-1})	k_{ex} (s^{-1})	$\overline{k_{ex}}$ (s^{-1})	Deviation (s^{-1})
6.41	93	421	375	398	32
6.83	93	726	708	717	13
7.045	93	820	965	893	103
7.45	93	947	1235	1091	204
8.01	98.5	1195	1212	1203	12

Table 3: The proton-exchange rate values of TmL complex (20 mM, 300 K), calculated with QUEST and omega plot methods.

4.4 Proton-exchange rate

The average of the k_{ex} values are shown in the next, summary table. It includes each measured molecule's results at each pH values and also their deviations.

Sample: TmL	Frequency: 93 ppm		Sample: ErL	Frequency: 48,5 ppm	
pH	k_{ex} (s^{-1})	Deviation (s^{-1})	pH	k_{ex} (s^{-1})	Deviation (s^{-1})
6.41	398	32	6.56	508	33
6.83	717	13	7.057	752	90
7.045	893	103	7.5	1042	64
7.45	1091	204	8.02	1204	277
8.01	1203	12			

Table 4: The proton-exchange rate values of TmL and ErL complexes (20 mM, 300 K), calculated with QUEST and omega plot methods.

It can be seen from the table that the proton-exchange rate values (k_{ex}) obtained with different calculation methods are quite similar. The two used methods are QUEST, which is concentration dependent and omega-plot, which is concentration independent. This underlines the fact that the measurements are reliable and confirms that only one isomer is present in the solution of ErL and TmL complexes. Furthermore, for both complexes the proton-exchange rate increases with the pH value, thus the kex (and so the CEST effect) is pH-dependent and the dependence can be described with the next equation [10].

$$k_{ex} = k_0 + k_a 10^{-pH} + k_b 10^{pH-pKw}$$

where k_0 is the spontaneous exchange rate, k_a is the acid-catalyzed exchange rate, and k_b is the base-catalyzed exchange rate.

In this case, the k_{ex} seems to depend mostly on the base-catalyzed exchange rate (k_b) as its value increases with the basic pH.

4.5 Outlook: Measurements after enzymatic cleavage

The demonstrated experiments were performed on the molecules before enzymatic cleavage (Figure 11). Measurements were made before in the team, on some of the molecules, after enzymatic cleavage, thus I can compare the results [13]. The enzymatic cleavage was not tested, they have synthesized the two molecules and tested them separately, which was to prove the concept first, and further on, do some enzymatic cleavage experiments with MRI.

Table 5 shows the difference between the frequencies of the CEST effects, in different molecules. LnL_1 is the molecule before enzymatic cleavage and LnL_2 is the one after (Figure 11) [13].

Two examples of the difference between the CEST spectra before and after enzymatic cleavage can be seen in Figure 19.

Lanthanide	Pr	Nd	Eu	Tb	Dy	Ho	Er	Tm	Yb
LnL_1 (ppm)	-	-	14	-107	-131	-59	48	93	42
LnL_2 (ppm)	-71	-33	-	-	-	-	-	-	-

Table 5: The frequencies of the CEST effects before and after enzymatic cleavage

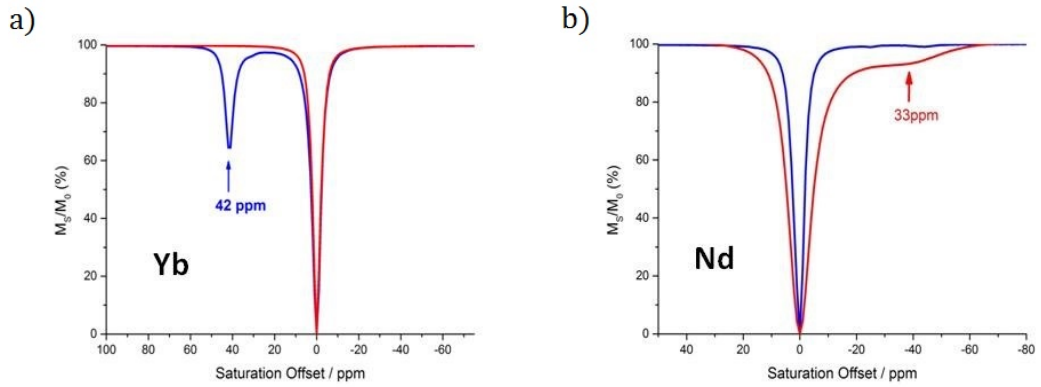

Figure 19: CEST spectra of YbL(a) and NdL(b) before(blue spectra) and after (red spectra) enzymatic cleavage (20 mM, pH 7.4, 300 K) [13]

The previous table and Figure 19 show that the model works, because a change in the CEST effect between the two states can be observed (a contrast is shown).

Similar experiments were performed in the team before [14] and also by Yuguo et al. in [15].

5 Conclusions

During my work, I studied eight different lanthanide complexes, which are potential MRI contrast agents. They were developed to detect amidase activity as PARACEST contrast agents, the measurements were performed to find out if they are capable of showing a contrast.

I investigated the PARACEST properties of the different lanthanides complexes of the molecule before enzymatic cleavage. This molecule comports only one labile proton on its structure so only one CEST effect was expected per complexes. Further examinations are needed on the state after enzymatic cleavage.

I measured the CEST spectra in a wide frequency range of each complexes. Six samples of the eight showed CEST effects, but PrL and NdL did not show any. For these two, previous studies showed that they have a CEST effect after enzymatic cleavage, so we also expect these complexes, to show a contrast. DyL and TbL have too small CEST effects, which cannot allow further examinations.

For further analysis, QUEST and QUESP measurements were performed on three complexes, at five different pH values (EuL, TmL and ErL). The EuL complex had three isomers of the molecule, the CEST signals were superimposed, so the proton-exchange rate cannot be calculated. For the other two samples (ErL and TmL), k_{ex} values were determined at different pH values. I have shown that reliable values of the proton-exchange rate were obtained using two different calculation methods (with small deviations). Furthermore for those two complexes, the k_{ex} value seems to depend on a base-catalyzed constant rate as the k_{ex} increases with the pH value.

I have studied in this work the effect of the lanthanide ions and the pH on the CEST effect of different complexes comporting the same chelating structure moiety. I have shown trough this work that the CEST effect is both lanthanide and pH-dependent, as they both affect the proton exchange rate constant. Furthermore, comparing the previous work to the one presented here showed that this molecules can be potential contrast agents, because of the changes in the CEST effects between the states before and after enzymatic cleavage. This change in the CEST effect will be translated into a change of the contrast in the MRI images.

Some enzymatic cleavage assays are planned in few months to check the ability of the amidase to cleave the substrate on the contrast agents. Some MRI picture will also be recorded to prove that the concept works.

Bibliography

[1] Anja Bockmann and Eric Guittet. Determination of fast proton exchange rates of biomolecules by NMR using water selective diffusion experiments. *FEBS letters, vol. 418, issuses 1-2 , pages 127-130*, 1997.

[2] Karsa Anita. *^{23}Na and ^{35}Cl NMR of saline solutions.* 2014.

[3] *http://mri-q.com/bloch-equations.html*, 2014.

[4] *http://spinwarp.ucsd.edu/neuroweb/Text/br-100.htm.*

[5] Carlos F. G. C. Geraldesa and Sophie Laurent. Classification and basic properties of contrast agents for magnetic resonance imaging. *Contrast Media Mol. Imaging, 4 1-23*, 2008.

[6] Elena Vinogradov, A. Dean Sherry, and Robert E. Lenkinski. CEST: From basic principles to applications, challenges and opportunities. *Journal of Magnetic Resonance, 229, 155-172*, 2013.

[7] Mark Woods, Donald E. Woessner, and A. Dean Sherry. Paramagnetic lanthanide complexes as PARACEST agents for medical imaging. *Chemical Society Reviews, 35, 500-511*, 2006.

[8] Byunghee Yoo and Marty D. Pagel. A PARACEST MRI Contrast Agent To Detect Enzyme Activity. *J. AM. CHEM. SOC., 128, 14032-14033*, 2006.

[9] Albert W. Overhauser. Polarization of nuclei in metals. *Phys. Rev. 92, 411*, 1953.

[10] Michael T. McMahon, Assaf A. Gilad, Jinyuan Zhou, Phillip Z. Sun, Jeff W. M. Bulte, and Peter C. M. van Zijl. Quantifying Exchange Rates in Chemical Exchange Saturation Transfer Agents Using the Saturation Time and Saturation Power Dependencies of the Magnetization Transfer Effect on the Magnetic Resonance Imaging Signal (QUEST and QUESP): pH Calibration for Poly-L-Lysine and a Starburst Dendrimer. *Magn Reson Med., 55, 836-847*, 2006 April.

[11] Thomas Chauvin, Susana Torres, Renato Rosseto, Jan Kotek, Bernard Badet, Philippe Durand, and Eva Toth. Lanthanide (III) Complexes That Contain a Self-Immolative Arm: Potential Enzyme Responsive Contrast Agents for Magnetic Resonance Imaging. *Chemistry, a European Journal, 18, 1408-1418*, 2012.

[12] W. Thomas Dixon, Jimin Ren, Angelo J. M. Lubag, James Ratnakar, Elena Vinogradov, Ileana Hancu, Robert E. Lenkinski, and A. Dean Sherry. A Concentration-Independent Method to Measure Exchange Rates in PARACEST Agents. *Magnetic Resonance in Medicine, 63, 625-632*, 2010.

[13] S. Laine, D. Agner, J. Mandel, J. He, T Chauvin, C.S. Bonnet, P. Durand, and E. Toth. Potential MRI contrast agent for enzymatic detection. *Poster presented at the 6th EucheMS conference on nitrogen ligands*, Spetember 2015.

[14] Thomas Chauvin, Philippe Durand, Michele Bernier, Herve Meudal, Bich-Thuy Doan, Fanny Noury, Bernard Badet, Jean-Claude Beloeil, and Eva Toth. Detection of Enzymatic Activity by PARACEST MRI: A General Approach to Target a Large Variety of Enzymes. *Angew. Chem. Int. Ed., 47, 4370-4372*, 2008.

[15] Yuguo Li, Vipul R. Sheth, Guanshu Liu, and Mark D. Pagel. A self-calibrating PARACEST MRI contrast agent that detects esterase enzyme activity. *Contrast Media Mol. Imaging, 6, 219-228*, 2011.